HHS Public Access

Author manuscript

Biomaterials. Author manuscript; available in PMC 2019 October 01.

Published in final edited form as:

Biomaterials. 2018 October ; 181: 126–139. doi:10.1016/j.biomaterials.2018.07.047.

Micropatterned cell sheets as structural building blocks for biomimetic vascular patches

Nae-Gyune Rim[1], **Alice Yih**[1], **Peter Hsi**[1], **Yunjie Wang**[2], **Yanhang Zhang**[1,2,3], **Joyce Y. Wong**[1,3,†]

[1]Department of Biomedical Engineering, Boston University, Boston, Massachusetts 02215

[2]Department of Mechanical Engineering, Boston University, Boston, Massachusetts 02215

[3]Division of Materials Science and Engineering, Boston University, Boston, Massachusetts 02215

Abstract

To successfully develop a functional tissue-engineered vascular patch, recapitulating the hierarchical structure of vessel is critical to mimic mechanical properties. Here, we use a cell sheet engineering strategy with micropatterning technique to control structural organization of bovine aortic vascular smooth muscle cell (VSMC) sheets. Actin filament staining and image analysis showed clear cellular alignment of VSMC sheets cultured on patterned substrates. Viability of harvested VSMC sheets was confirmed by Live/Dead® cell viability assay after 24 and 48 hours of transfer. VSMC sheets stacked to generate bilayer VSMC patches exhibited strong inter-layer bonding as shown by lap shear test. Uniaxial tensile testing of monolayer VSMC sheets and bilayer VSMC patches displayed nonlinear, anisotropic stress-stretch response similar to the biomechanical characteristic of a native arterial wall. Collagen content and structure were characterized to determine the effects of patterning and stacking on extracellular matrix of VSMC sheets. Using finite-element modeling to simulate uniaxial tensile testing of bilayer VSMC patches, we found the stress-stretch response of bilayer patterned VSMC patches under uniaxial tension to be predicted using an anisotropic hyperelastic constitutive model. Thus, our cell sheet harvesting system combined with biomechanical modeling is a promising approach to generate building blocks for tissue-engineered vascular patches with structure and mechanical behavior mimicking native tissue.

[†]For correspondence. Tel.: +1-617-353-2374. Fax: +1-617-353-6766. jywong@bu.edu.

Author contribution

N.R. designed, planned and performed the experiments. A.Y. assisted cellular experiment. P.H. (Y.W assist) performed computational modeling study with Y.Z. supervision. J.Y.W. supervised the overall research. All authors discussed the progress and reviewed the manuscript.

Conflicts of interest

None.

Appendix A. Supplementary data

The following is the supplementary data related to this article:

Figure S1-S6.

Data availability

All experimental data required to reproduce the findings from this study will be made available on request.

Keywords

Cell sheet; hydrogel; vascular smooth muscle cell; tensile testing; patterning; finite element modeling

1. Introduction

A major goal in tissue engineering is to develop biomaterials that mimic the biomechanical characteristics of native tissue [1–3]. In vascular tissue engineering, a biomimetic approach is critical because mismatch of hierarchical structure and mechanical properties between native and tissue-engineered implants can cause complications negatively impacting regeneration and remodeling [4–6]. To avoid these complications, it is important to understand relationships between the complex structure and mechanical properties in the context of vessel function [7, 8]. Vascular smooth muscle cells (VSMCs) are highly specialized cells with primary function of contraction and blood flow regulation [9]. In a native blood vessel, VSMCs align circumferentially to form the medial layer of arteries and provide structural support, contractility, and vessel elasticity [10]. In addition, the medial layer is composed of multilayers of highly ordered VSMCs and extracellular matrix (ECM) that are arranged in distinct helical configurations [11–13]. Several reports have shown correlations between structural organization of cells and ECM and function of vascular constructs, i.e. proteins such as fibronectin, elastin, and collagen play an important role in controlling structural integrity [14–16]. Aligned VSMCs in the medial layer play an important role to maintain vascular tone and actively regulate blood pressure through contraction/relaxation and change in arterial diameter, which together influence mechanical properties of the arterial wall [17].

The mechanics of native arterial wall are known to have nonlinear and anisotropic stress-strain behavior [18]. While the arterial wall is compliant in the low range of strain, collagen gradually begins to bear the load as strain increases, which results in the arterial wall stiffening (nonlinearity) [19, 20]. The uniaxial tensile stress-stretch responses show that the mechanical response of the arterial medial layer in a circumferential direction tends to be stiffer than in a longitudinal direction (anisotropy) [21]. There is a strong relationship between the cells' complex helical arrangement and ECM around the circumference of the vessel; each elastic lamellae in the medial layer alternates with a layer of smooth muscle cells, collagen fibers and together, collectively organizing into a lamellar unit considered to be the functional unit of the vessel wall [22, 23]. Therefore, it is clear that developing tissues with defined structure that mimics that of a native vessel is key for successful tissue-engineered vascular grafts [24]. Further, we have reported previously that characterization of the mechanical properties of VSMC layers combined with computational modeling could be a valuable strategy to provide insight and to predict the mechanical properties of engineered blood vessels, which would be an invaluable tool set to help prioritize the overwhelming number of design options [25].

Bottom-up tissue engineering approaches aim to create biomimetic engineered tissue by recreating the microstructural features of tissues, while traditional top-down approaches, in

which cells are seeded on polymeric scaffold, often have difficulty to control the tissue microstructure [26, 27]. As one of bottom-up approach, cell sheet engineering has progressed rapidly in the past decade and has emerged as a novel approach for scaffold-free, cell-based therapy [28]. Cell sheet technology, based on cells producing their own ECM [29], allows for viable, transplantable cell sheets for various tissue engineering applications [30, 31]. It also involves building three dimensional layer-by-layer from monolayer cell sheets composed of cells and their ECM [32, 33]. To recreate the microstructural features of tissues, micropatterning technology via photolithography have been combined with cell sheet engineering strategy using microgroove textured elastomeric substrates to provide topological cues [34–36], using elastomeric microcontact pattern printing to print the cell adhesive pattern on the substrate surface [37], or using cyclic mechanical stretching to guide cellular alignment [38]. Previous work from us and others has showed micropatterned substrate-guided cellular alignment and improved aspect ratio of VSMCs [22, 39], as well as nonlinear and anisotropic mechanical behavior in aligned VSMC sheets [24, 40]. However, in a bottom-up approach, bridging the gap between individual aligned cell sheets to tissue-like three dimensional multi-layered patches has yet to be characterized.

To achieve non-invasive release of intact cell sheets from underlying substrates, various stimuli systems have been reported, such as temperature, enzyme, electricity, and magnetic field. [30, 41, 42]. Here, we use enzymatically degradable cellulose- or alginate-based hydrogels: these substrates are conjugated with tyramine in order to enable crosslinking between chains via phenol moieties using Horseradish peroxidase (HRP) [43–46]. Cellular adhesion and proliferation of fibroblasts first were confirmed on hydrogel substrates with varying phenol hydroxyl group content [47], peroxidase or H_2O_2 concentration [48], and a simple feasibility test of tyramine-conjugated cellulose for cell sheet applications has been reported [49]. Recently, we have further developed and optimized this system to generate multi-layer cell sheets [50, 51]. Briefly, tyramine-conjugated alginate (Alty) or carboxymethyl-cellulose (CMCty) act as sacrificial substrates for cell sheet-based harvest and transfer system and do not compromise mammalian cells or ECM during the enzymatic degradation process of the underlying hydrogel substrate.

In this study, we fabricated aligned VSMC sheets to mimic the structure of cells in the native arterial medial layer. A surface-patterned degradable hydrogel substrate was used to produce patterned VSMC sheets that were subsequently stacked in alternating angles to make patches that mimic the multilayer structure of the medial layer in an artery. First, we analyzed the effect of surface patterning on the monolayer VSMC sheet cellular alignment. The morphology and cellular structure of VSMC sheets grown on patterned and nonpatterned hydrogel were observed, and their contractile marker expression was compared. After the VSMC sheets were harvested from the substrate, their cellular structure and viability were characterized. The mechanical properties of the harvested VSMC sheets were also characterized to determine the effect of patterning on mechanical non-linearity and anisotropy, which are known characteristics of native blood vessel walls. We also developed a strategy to stack VSMC sheets into bilayer VSMC patches without damaging their structure and confirmed strong bonding between the two layers of VSMC sheets. The structure of bilayer VSMC patches was characterized by pre-labeling each layer prior to stacking, and collagen content was characterized by staining and was quantified by standard

assays. Moreover, patterned VSMC sheets were stacked in alternating angles mimicking the structure of native vessels. A finite-element model was developed to investigate the effect of geometric design parameters on the tensile mechanical response of the bilayer VSMC patches.

2. Materials and methods

2.1. Materials

2-(N-morpholino)ethanesulfonic acid (MES) was purchased from Alfa Aesar™ (Tewksbury, MA, USA); Krebs-Ringer Bicarbonate Buffer solution (Krebs) from Biotang Inc. (Lexington, MA, USA); human plasma fibronectin from MilliporeSigma (Bedford, MA, USA); and collagen type 1 rat tail from Corning Inc. (Corning, NY, USA). Low glucose Dulbecco's modified Eagle medium (DMEM), Fetal bovine serum (FBS), 0.05% trypsin-0.48 mM ethylenediaminetetraacetic acid (EDTA), 100x antibiotic-antimycotic (ABAM), 100x L-glutamine (200 mM), and phosphate-buffered saline (PBS) were purchased from Gibco BRL (Gaithersburg, MD, USA). Polydimethylsiloxane (PDMS) from Dow Corning (SYLGARD® 184 Silicone Elastomer Kit, Midland, MI). Unless otherwise specified, all other chemicals and solvents were obtained from Sigma (St. Louis, MO, USA).

2.2. Hydrogel substrate preparation

As shown in Table 1, tyramine-conjugated carboxymethyl cellulose (CMCty) and alginate (Alty) were synthesized based on the method previously reported with some modification [48, 49]. Briefly, carboxymethylcellulose sodium salt (Medium viscosity) or alginate sodium salt were dissolved in MES buffer with stirring overnight, then tyramine hydrochloride was added. The next day, NHS (N-hydroxysuccinate), HOBt (1-Hydroxybenzotrizole hydrate) and EDC (N-(3-Dimethylaminopropyl)-N′-ethyl carbodiimide hydrochloride) were added. After 24 hours of gentle stirring at room temperature, the polymer solution was transferred to Slide-A-Lyzer™ Dialysis Cassette G2 (Thermo Fisher Scientific, Waltham, MA, USA) and dialyzed against distilled water (2 L) for 48 hours with the distilled water being changed every 12 hours. The washed sample was frozen in a deep-freezer (−80°C) overnight, lyophilized, and stored in a −20°C freezer. The lyophilized material was dissolved in Krebs buffer (1.5 wt%) with gentle magnetic bar stirring and filtered with 1μm pore size syringe filter before use.

To generate micropatterned topographical cues on the hydrogel substrate, patterned PDMS and gelatin molds were used as patterned stamps (Scheme 1). The patterned stamps were generated using a silicon wafer master made using photolithography [52]. Briefly, a 5 μm thick negative photoresist layer (SU8–5, Microchem, Newton, MA, USA) was spin-coated onto silicon wafers and soft-baked at 65°C and 95°C. UV light was filtered through a patterned mask containing multiple parallel lines (30 μm wide and spaced) to expose the photoresist layer selectively. After exposure, the silicon wafer was developed in the developer solution to remove un-crosslinked photoresist. This procedure created a patterned silicon wafer master that could be used to generate multiple patterned PDMS. A mixture of PDMS (base: curing agent = 10:1) was poured against the master, followed by 5 min vacuum degassing, and cured in an 80°C oven overnight. The cured patterned PDMS mold

was peeled off and cut into circular (diameter: 26 mm) or rectangular shapes (20 mm x 20 mm). A nonpatterned PDMS mold was created against a flat normal culture plate. PDMS molds were washed with 70% EtOH and sterilized in cell culture hood under UV light for 30 min. The sterile PDMS was put on a culture plate (pattern on up), then a warm type B gelatin solution (10 wt% in PBS, 0.02 μm filtered) was poured over it. The plate sealed with Parafilm was cooled to 4°C to solidify the gelatin. The gelatin mold was cut, peeled off, flipped over to a new plate, and stored at 4°C before use, to prevent melting.

To make hydrogel substrates, 1ml of 1.5 wt% Alty or CMCty was mixed well with 1 μl HRP (1 unit/μl in Krebs) before filling the gelatin mold, followed by layering a dialysis membrane on top. This was further cross-linked by adding a hydrogen peroxide solution (0.15 wt% in Krebs) on top of the dialysis membrane and kept at 4°C for 30 min. Once the hydrogel was polymerized, the layer of dialysis membrane was peeled off, warm PBS added, and the plate gently swirled to melt the gelatin mold. This was followed by several rinses with fresh PBS to completely wash out the gelatin. To confirm the pattern maintenance via stamping method among different molds, microscopic images were taken for the PDMS, gelatin mold, and hydrogel substrate (Scheme 1c).

Bovine aortic VSMCs (Coriell Cell Repositories, Camden, NJ, USA) were cultured in low glucose DMEM supplemented with 10 % FBS, 1× ABAM, 1 mM L-glutamine. Cells were initially seeded in 5×10^4 cells/cm^2 density on collagen type 1- (10 μg/ cm^2) or fibronectin- (10 μg/cm^2) coated nonpatterned (random) or patterned hydrogel substrates. Once cells reached 80% confluence, the culture medium was supplemented daily with 50 μg/ml L-ascorbic acid.

2.3. Cellular morphology and orientation analysis

After 7 days of culture, cells were fixed with 4% paraformaldehyde in PBS for 10 min and permeabilized with 0.5% Triton X-100 in PBS for 15 min. Samples were incubated in a blocking buffer (1% bovine serum albumin in PBS) at 37°C for one hour. The samples were counter-stained with 1:200 rhodamine-phalloidin (Life Technologies, Woburn, MA, USA) and 1:5000 Hoechst (Invitrogen, Carlsbad, CA, USA) in blocking buffer at 37°C for one hour. Images for each sample were captured using fluorescence microscopy (Axiovert S100, Carl Zeiss Microscopy LLC, Thornwood, NY, USA). To quantify cellular alignment, images were further processed to analyze cellular orientation within sheets via two-dimensional fast Fourier transform (2D FFT) and the ImageJ Oval Profile plug-in, as previously described [33, 38].

2.4. Contractile and synthetic phenotype marker expression

After 7 days of culture, cells were washed twice with PBS, and mRNA was isolated from the cell/substrate construct by using QIAshredder and RNeasy Plus Mini Kit (Qiagen, Hilden, Germany). cDNA synthesis was performed using a High Capacity RNA-to-cDNA Kit (Applied Biosystems, Thermo Fisher Scientific, Waltham, MA, USA). Quantitative PCR (qPCR) amplification was completed using a TaqMan Gene Expression Master Mix and TaqMan primer sets (Applied Biosystems, Thermo Fisher Scientific, Waltham, MA, USA). Relative gene expression of cell/substrate constructs was compared with that of nonpatterned

cell sheets, which were considered as controls, using the delta delta Ct (ddCt) method. Glyceraldehyde 3-phosphate dehydrogenase (GAPDH) was used as a housekeeping gene to normalize expression levels of four contractile phenotype markers and three synthetic phenotype markers [53, 54]. The chosen contractile phenotype markers were smooth muscle alpha-actin (ACTA2), smooth muscle myosin heavy chain 11 (MYH11), transgelin smooth muscle protein 22-alpha (TAGLN), and smooth muscle calponin (CNN1). Vimentin (VIM), non-muscle myosin heavy chain 10 (MYH10), and tropomyosin 4 (TPM4) were chosen as the synthetic phenotype markers.

After 14 days of culture, cells were fixed with 4% paraformaldehyde in PBS for 10 min and permeabilized with 0.5% Triton X-100 in PBS for 15 min. Samples were blocked in a blocking buffer (1% bovine serum albumin in PBS) at 37°C for one hour. Samples were further stained by sequential incubation with rabbit polyclonal anti-smooth muscle myosin heavy chain 11 (MYH11) primary antibody (1:200, ab53219, Abcam, Cambridge, UK) for one hour, and Alexa Fluor® 568 Donkey Anti-Rabbit IgG secondary antibody (1:100, A10042, Life Technologies, Woburn, MA, USA) with Hoechst (1:5000) for one hour. The images were taken using z-stacking in a confocal microscope (IX81, Olympus Corporation, Shinjuku, Tokyo, Japan).

2.5. Harvesting VSMC sheets and their viability

To harvest and transfer the cell sheet to another substrate, the surface of the cell sheet and the new substrate were coated with collagen or fibronectin in serum-free media for 30 min. As shown in Figure 1a, the cell sheet/hydrogel substrate construct was flipped over onto the new normal cell culture plate and incubated for one hour in a culture medium to allow cell sheets to adhere to the new plate. 5U/ml of cellulase (0.2mg/ml for alginate lyase) was added into the culture medium for one to two hours at 37°C to degrade the hydrogel. After the substrate was degraded, we added fresh medium to stabilize the cell sheet for further analysis or culture.

To evaluate survival efficacy of the harvested cell sheet, we used the Live/Dead® cell viability assay (Life Technologies, Woburn, MA, USA), which distinguishes live from dead cells by simultaneous staining with green-fluorescent calcein-AM to indicate intracellular esterase activity, and red-fluorescent ethidium homodimer-1 to indicate loss of plasma membrane integrity. After aspirating the medium, the cell sheet was washed once with PBS then incubated with the staining solution (5 μL calcein AM and 20 μL ethidium homodimer-1 in 10 mL PBS) for 30 min at room temperature. Then the cells were observed through a fluorescence microscope. The viability study was performed after hydrogel degradation, 24 hours and 48 hours after the cell sheet was transferred onto normal culture plates. Images for each sample were captured using fluorescence microscopy. The images were further processed using ImageJ to count and normalize viable cells within harvested cell sheets.

2.6. Bilayer VMSC patch fabrication

The strategy for obtaining multiple layer cell sheets is similar to the cell sheet transfer/harvest procedure (Figure 1b). While only CMCty was used for monolayer VSMC sheet

fabrication, CMCty and Alty were both needed to fabricate bilayer VSMC patches, and Alty was selectively degraded after stacking. After 9 days of culture, the VSMC sheet cultured on Alty was gently transferred on top of another VSMC sheet cultured on CMCty. After 1 hour of incubation, alginate lyase (0.2mg/ml alginate lyase in culture medium) was added for 2 hours at 37°C to degrade the top layer hydrogel substrate (Alty), resulting in bilayer VSMC patches supported on CMCty. Then, the stacked VSMC sheets were incubated overnight to promote interactions to stabilize the construct as bilayer VSMC patches. To visualize the cell sheets within the bilayer VSMC patches, each layer was pre-labeled with cell tracker® (Green CMFDA, Red CMPTX, Invitrogen, Carlsbad, CA, USA) prior to stacking.

To confirm if overnight incubation is enough to form a strong interaction between layers in bilayer VSMC patches, we performed a lap shear test using a custom uniaxial tensile tester [55]. Once the pre-labeled cell sheet/hydrogel constructs were prepared, one cell sheet/hydrogel construct was flipped over and partially stacked on the other cell sheet with a hydrogel construct back and incubated overnight. Each hydrogel were gently glued to transparent film frames using Loctite® 414 super bonder instant adhesive (Henkel, Corporation, Westlake, OH) and then mounted on the tensile tester. The partially-stacked VSMC sheets were stretched using the uniaxial tensile tester to characterize the detachment between the layers. Cell sheets stacked immediately before stretching (0 hour incubation) were used as a control group.

To generate ‘bilayer tilted patterned’ VSMC patches (BTP), patterned VSMC sheets were stacked in alternating angle with bottom layer (+15°) and top layer (−15°) aligned relative to X direction as shown in Figure 1c. The angle was decided based on previous report showing 3D confocal imaging of aortic medial layer [56]. For parallel alignment stacking, both bottom and top patterned VSMC sheets were stacked in parallel to X direction to generate ‘bilayer parallel patterned’ VSMC patches (BPP). ‘Bilayer nonpatterned’ VSMC patches (BNP) were stacked in arbitrary direction.

2.7. Collagen content and structure characterization

To measure collagen content, cell sheets grown on hydrogel substrates in 12-well culture plates were harvested by enzymatically degrading the hydrogel. The harvested cell sheets were rinsed with 1× PBS, and their wet mass was measured after lightly tapping on Kimtech wipes to minimize extra water in the sample. The samples were incubated at 4°C in 0.1mg/ml porcine pepsin and 0.5M acetic acid for 24 hours. The acid-soluble and pepsin-soluble collagen content were measured using Sircol™ soluble collagen assay (Biocolor Ltd., Carrickfergus, County Antrim, United Kingdom) following the manufacturer’s protocol. Briefly, samples were prepared in 100 μl volume of 0.5M acetic acid, and 1ml of Sircol Dye Reagent was added to saturate the collagen molecules. The samples were gently shaken for 30 min and centrifuged at 12,000 rpm for 10 min. After removing supernatant, 750 μl ice-cold Sircol Acid-Salt Wash Reagent was added and centrifuged at 12,000 rpm for 10 min. The supernatant was removed and 250 μl Sircol Alkali Reagent was added. After 30 min, 200 μl of each sample (including blank and standards), was transferred to a 96-well plate and absorbance was measured at 555 nm. To visualize collagen type 1 within a cell sheet, cells were stained following the same procedure previously described using rabbit

polyclonal anti-collagen type 1 primary antibody (1:200, ab34710, Abcam, Cambridge, UK) instead.

To examine collagen structure of VSMC sheets, cells were fixed with 4% paraformaldehyde in PBS for 10 min and permeabilized with 0.5% Triton X-100 in PBS for 15 min. Samples were blocked in a blocking buffer (1% bovine serum albumin in PBS) at 37°C for one hour. Samples were further stained by sequential incubation with rabbit polyclonal anti-collagen primary antibody (1:200, ab34710, Abcam, Cambridge, UK) for one hour and 568 Donkey Anti-Rabbit IgG secondary antibody (1:100, Life Technologies, Woburn, MA, USA) with Hoechst (1:5000) for one hour. Images were taken using z-stacking in a confocal microscope.

2.8. Mechanical characterization

2.8.1. Uniaxial tensile testing—To characterize mechanical behavior of monolayer and bilayer cell sheets, a custom-built uniaxial tensile tester was used [55]. Monolayer VSMC sheets were cultured on rectangular shaped substrates for 14 days. The thickness (T_o) of VSMC sheets were measured using an optical microscope, and then the cell sheets were harvested by degrading the hydrogel using cellulase or alginate lyase within the medium. Edges of VSMC sheets were glued to transparent film frames using Loctite® 414 super bonder instant adhesive and then mounted on the tensile tester. To characterize anisotropic mechanical behavior of monolayer cell sheets, patterned VSMC sheets (P) were mounted in the direction of alignment (parallel, P (∥)) or the direction perpendicular to alignment (P (⊥)), while nonpatterned VSMC sheets (NP) were mounted in arbitrary directions. Before collecting data, VSMC sheets were manually stretched to the point where they began to bear load and their initial width (W_0) and length (L_0) were measured. The samples were also pre-conditioned by performing three pre-stretch load cycles to 20% stretch. VSMC sheets were mechanically characterized by stretching samples to failure at a strain rate of 3.33% s^{-1}. Force (F) and deformed length (L) was acquired from the uniaxial tensile tester, and then used to calculate Cauchy stress (σ) and stretch (λ), assuming incompressibility.

$$\sigma = \frac{F}{A} = \frac{F}{A_0} \cdot \frac{L}{L_0} = \sigma_e \cdot \lambda \quad (1)$$

$$\lambda = \frac{L}{L_0} = \varepsilon + 1 \quad (2)$$

where σ_e and ε are engineering stress and strain, A_0 is the undeformed cross-sectional area and $A_0=W_0T_0$.

Failure stress (Max Stress) and failure stretch (Max Stretch) were measured, and modulus was determined over the linear regime of the stress-stretch curve. Similar to the method reported by Backman et al. [40], two linear regimes was chosen to calculate the tangent modulus for mechanical nonlinearity quantification of VSMC sheets. Initial 10% (0%~10%)

of total stretch was chosen for low stretch range and final 10% (90~100%) of total stretch was chosen for high stretch range tangent modulus analysis.

For mechanical characterization of bilayer VSMC patches, patterned VSMC sheets were stacked in parallel to generate BPP, and were stretched in directions where θ was 0° or 90°. Patterned VSMC sheets were also stacked in alternating angle to generate BTP, and were stretched in directions where θ was 15° or 75°.

2.8.2. Finite element modeling—A finite element model was developed in Abaqus 2017 (Dassault Systèmes Simulia Corp, Johnston, RI, USA) to simulate the uniaxial tensile testing of bilayer VSMC patches [57]. Bilayer cell sheets were represented by two collagen fiber families orientated in a specific direction and surrounded by a non-collagenous isotropic ground material. The strain energy density function of this constitutive model is given by [57] :

$$\psi = C_{10}(\bar{I}_1 - 3) + \frac{k_1}{2k_2}\sum_{a=1}^{N}([exp\{k_2(\kappa(\bar{I}_1 - 3) + (1 - 3\kappa)(\bar{I}_4 - 1)^2)\} - 1] \quad (3)$$

where $C_{10} > 0$, $k_1 > 0$, are stress-like material parameters and $k_2 > 0$ is a dimensionless parameter. The first term in Equation (3) is associated with the non-collagenous matrix of the material and described by an isotropic Neo-Hookean model, whereas the second term in Equation (3) is associated with the anisotropic contribution of collagen to the overall response. Parameter κ $\left(0 \le \kappa \le \frac{1}{3}\right)$ characterizes collagen fiber dispersion. In this study, we set $\kappa = 0$, which describes the case where all fibers are perfectly aligned ($\kappa = 1/3$ when the fibers randomly dispersed). The function also includes $\bar{I}_4$, defined as:

$$\bar{I}_4^{\,2} = \lambda_1^2\cos^2\theta + \lambda_2^2\sin^2\theta \quad (4)$$

where θ is the angle between the direction of the patterning and the direction of stretching, so that the angle between two collagen fiber families, or the angle between two patterned VSMC sheets in the experiment, is 2θ (Figure 1c).

A bilayer VSMC patch sample with an approximate size of 5.5 mm x 4 mm was modeled, and general purpose shell elements (S4R) were used. Boundary conditions were applied in accordance to the experimental uniaxial tensile testing. The left surface edge was fixed, while the right surface edge was bounded and allowed to deform in x-direction with an applied edge force of 0.005 N/mm. Cauchy stress and stretch data were obtained from an element located at the center of the object in order to avoid boundary effects. The model parameters were adjusted to fit the experimental data (θ = 0°) of bilayer patterned VSMC patches (BP), which were $C_{10} = 0.0025$, $k_1 = 0.00038$, and $k_2 = 0.0028$. The same set of model parameters were then used to predict the stress-stretch behavior of other BPs with different patterning angles (θ = 15°, 75°, 90°) by changing θ according to the cell sheet patterning direction while keeping all other parameters the same. To assess the goodness-of-

fit and model prediction, a root-mean-square (RMS) measure of error was calculated as [58, 59]:

$$RMS = \sqrt{\frac{\sum_1^n (\sigma_E - \sigma_M)^2}{n}} \quad (5)$$

where σ_E and σ_M are Cauchy stress from the experiment and model, respectively, and n is the number of data points.

3. Results and Discussion

3.1. Patterned substrate regulates cellular organization of VSMC sheets

To understand the effect of micropatterned hydrogel substrate on VSMC sheet alignment, VSMCs were seeded onto patterned and non-patterned hydrogel substrates. Microscopic images were taken during culture to observe the initial adhesion and proliferation of VSMCs to form confluent VSMC sheets on the hydrogel substrate (Figure S1). As shown in Figure 2a, VSMCs grown on the nonpatterned substrates showed randomly oriented morphology throughout the culture period while cells grown on the patterned substrate appeared elongated along the direction of the hydrogel substrate patterns. To better observe the cytoskeletal structure of the cells, we stained VSMC actin filaments using tetramethylrhodamine (TRITC)-conjugated phalloidin. F-actin filament staining showed different morphologies for cells grown on each substrate. Aligned VSMC sheets on the patterned surface exhibited a more spindle-like morphology than on the nonpatterned surface, in which the VSMCs displayed a random cellular direction. To better understand the cellular orientation within the VSMC sheet, we used two-dimensional fast Fourier transform (2D FFT) to further analyze the actin filament stained images. As shown in Figure 2b, we observed strong intensity in the direction of the substrate patterns for the patterned VSMC sheet, while the nonpatterned VSMC sheet did not show a specific direction but rather showed arbitrary orientations, which was similar to other studies using the same cell type on PDMS as a substrate [22, 34, 40]. The patterned VSMC sheets showed the highest peak of 4.81 at 0°, which is the direction of the substrate pattern. The nonpatterned VSMC sheet showed intensity of 1.22 at 0° with similar intensity oriented in the other direction, indicating random orientation. Most cell types are known to orient and move along fibers with a range of 5~50 μm in diameter [22, 60]. The data presented in this study for patterned VSMC sheets are based on substrates that have 30 μm width/spacing and 5 μm depth of multiple parallel grooves. The preliminary screening with various dimensions of width/spacing from 10 μm to 50 μm showed no difference in alignment and showed similar results for orientation distribution (data not shown). This agrees with findings from Sarkar *et al.* that VSMCs are aligned with their long axis parallel to the micropatterned PDMS substrates, showing no significant differences among various pattern groove width [22]. Sarker *et al.* reported 95% VSMC alignment on 19, 48 and 79 μm patterned substrates, while non-patterned substrates showed 15% alignment. While preliminary screening showed similar alignment, upon further cell culture, we observed that the 50 μm patterned group showed locally less alignment in magnified view. In contrast, the 10 μm patterned group was locally

well-algined, but did not reach 100% confluence to form a cell sheet. This led us to choose 30 μm patterned group for further study.

To assess if there is a cellular alignment effect on the contractile phenotype expression of VSMC sheets, quantitative TaqMan real-time polymerase chain reaction (qPCR) analysis was performed (Figure 3a and S2). Four markers were selected for the contractile phenotype profile, and the patterned VSMC sheet showed two- to three-fold higher expression relative to the nonpatterned VSMC sheet. Many of these genes are known to be involved in VSMC contraction, either as a structural component of the contractile apparatus or as a contraction regulator [53]. Patterned VSMC sheets showed 2.8 ± 0.2 fold of ActA2, 1.9 ± 0.2 fold of MYH11, 1.9 ± 0.06 fold of TAGLN and 1.8 ± 0.04 fold of CNN1 expression relative to nonpatterned VSMC sheets. In another report, Lee et al. [38] also reported contractile phenotype gene expression analysis for VSMC sheets. It also showed upregulated contractile phenotype expression of patterned VSMC sheets relative to nonpatterned VSMC sheets, showing about 1.1 fold of α-SMA and 1.4 fold of calponin gene expression. Interestingly, TaqMan PCR for RNA isolated from bovine aorta showed more than 50-fold of higher expression for all contractile phenotype genes shown in this study (data not shown), while patterned VSMC sheets showed 1.8~2.8 fold of expression level relative to nonpatterned VSMC sheets. Here, we have also showed downregulated synthetic phenotype expression of patterned VSMC sheets relative to nonpatterned VSMC sheets (Figure S2). It is known that *in vitro* VSMCs undergo phenotypic dedifferentiation to the synthetic phenotype and lose their contractile phenotype after serial passages [9, 39, 61, 62]. As the VSMCs used for the cell sheets was passage 10 to 12, the VSMCs had already lost the contractile phenotype, which explains the relatively low expression level compared to native aorta. Several studies have shown that the VSMCs cultured on patterned substrates increased contractile phenotype expression. Previously, SMCs alignment induced by aligned fibers showed stronger α-SMA expression especially during longer culture periods [63]. Genomic profiling and protein expression of primary rat aortic SMC cultured on flat and micropatterned substrates showed lower proliferation but higher differentiation (contractile phenotype) on cells cultured and passaged on micropatterned substrate [39]. However there have been no previous reports on cell phenotype within cell sheets. In this study, we found that the patterning has minimal effect on cell sheet's phenotypic level, showing relatively small fold of gene expression level change compared to elsewhere [39, 63]. We have also confirmed positive staining of the contractile phenotype marker protein MYH11 by staining both nonpatterned and patterned VSMC sheets, of which the latter was more organized and slightly stronger (Figure 3b). Therefore, the patterning has more effect on cellular structure of the cell sheet, rather than on protein composition.

3.2. Harvesting VSMC sheets and their characterization

To probe the harvest/transfer strategy of VSMC sheets from the hydrogel substrate in response to enzymatic degradation, VSMC sheets were prepared on a circular-shaped hydrogel substrate. The harvested and transferred VSMC sheet on culture plate was observed via microscope to compare the cellular structure of the sheet before and after transfer (Figure 4a). The result showed that the circular VSMC sheet was completely transferred from the circular hydrogel to the flat culture plate and that the aligned structure

of the patterned VSMC sheet was maintained after transfer. We verified cellular efficacy of harvested VSMC sheets from Live/Dead® cell viability assay images (Figure 4b); moreover, the bottom panels show maintenance of cellular organization in patterned VSMC sheets. Most of the cells were confirmed to be alive for all groups, as labeled by green fluorescence, and relatively few cells were stained red, which indicates dead cells. NP showed 98.05 ± 0.32 % (24 hours), 98.21 ± 0.14 % (48 hours) viability and P showed 98.18 ± 0.46 % (24 hours) and 98.81 ± 1.23 % (48 hours) viability. These results showed that the cell sheet harvest strategy using a degradable hydrogel as a sacrificial substrate supported the cellular structure maintenance and viability of an intact cell sheet for at least 48 hours. Sakei et al. showed reattachment of L929 cell sheets released from hydrogels and transferred to cell culture dishes with 96.8% viability [48, 49]. However the cellular organization of the reattached L929 cell sheet was not tested. In this study, we have shown that the cellular structure of patterned VSMC sheets was maintained after harvest/transfer process with good cellular viability using a stamping method. Jun et al. reported the transfer of patterned cell sheets using a similar stamping method on a thermoresponsive system showing pattern maintenance and cell viability, but only immediately after the transfer process [35]. Here, we have shown a viable and structurally maintained patterned cell sheet over an extended incubation period (after 24 and 48 hours of transfer). It is important for the cell sheets to maintain their patterning after release to generate multiple layers of patterned cell sheets for implanted vascular patches. As the complete stacking procedure (stack, incubate, hydrogel degradation) of one layer takes 4~6 hours and the pattern maintenance of harvested cell sheet was confirmed for 24 and 48 hours, this suggests the potential of our system's capability of generating multiple layers of patterned cell sheets while maintaining the pattern.

To determine effects of cellular organization in VSMC sheets on mechanical properties, VSMC sheets were harvested after two weeks of culture. Cauchy stress-stretch responses for patterned and nonpatterned VSMC sheets are shown in Figure 5. It is important to note that engineering stress significantly underestimated the stress in the cell sheet due to large deformation, as shown in Equation 1 (Figure S3). To quantify the anisotropic mechanical behavior, patterned VSMC sheets were tested in both directions, either parallel (P (∥)) or perpendicular (P (⊥)) to the stretching direction. As Figure 5a shows, both patterned and nonpatterned VSMC sheets showed nonlinear stress-stretch behavior. Parallel stretching (P (∥)) showed stiffer behavior than perpendicular stretching ((P (⊥)), indicating anisotropic mechanical behavior of patterned VSMC sheets. The stress-stretch curve was further analyzed to calculate stretch at failure (Max Stretch), stress at failure (Max Stress), and modulus at low and high stretch range (Figure 5b and c). Patterned VSMC sheets showed lower max stretch and higher max stress in parallel stretching than perpendicular stretching, which indicates stronger stiffness of parallel patterned VSMC sheets. By comparing modulus in low stretch range (initial of total stretch) and high stretch range (end of total stretch), an increase of modulus for all VSMC sheets was shown in high stretch range compared to low stretch range, which is a characteristic of mechanical non-linearity. The degree of mechanical anisotropy of VSMC sheets can be confirmed by comparing the ratio of the mechanical properties in the aligned (parallel) direction relative to the perpendicular direction in Figure 5c. Patterned VSMC sheets showed max stretch ratio as 0.61 ± 0.04, max

stress ratio as 1.31 ± 0.07, modulus ratio in low stretch range as 1.39 ± 0.12 and modulus ratio in high stretch range as 2.22 ± 0.13, which indicates mechanical property dependence on the patterning direction. Meanwhile nonpatterned VSMC sheets showed the values of the ratios as 1.00 ± 0.05 (max stretch), 1.07 ± 0.25 (max stress), 1.14 ± 0.39 (modulus ratio in low stretch) and 1.02 ± 0.15 (modulus ratio in high stretch), indicating isotropic mechanical behavior. Also, VSMC sheets cultured without ascorbic acid resulted in much weaker mechanical properties (results not shown), and it was challenging to harvest intact cell sheets. Ascorbic acid treatment produces ECM-rich sheets, which resulted in 5- to 10-fold of stiffness increase and further improved the mechanical integrity of cell sheets. Previous work within our lab has shown that the VSMC sheets grown on thermo-responsive pNIPAAm grafted PDMS substrate show 208~250 kPa stiffness (modulus), which is relatively higher than what we reported here [40]. The culture period may have played a role, as cell sheets on pNIPAAm-PDMS were cultured 17~21 days with daily ascorbic acid treatment in the previous report, while cell sheets were cultured 14 days in this study. We note that in previous report of our laboratory, VSMC sheets reached the MPa range stiffness (5.77~8.95 MPa stiffness in modulus) by being cultured for a much longer period, 10 weeks, to guide spontaneous cell sheet release [24]. Our findings here are consistent with the idea that culture period is an important factor for generating strong, mature cell sheets. In this study, patterned VSMC sheets showed mechanical nonlinearity and anisotropic behavior which is an important characteristic as a biomimetic approach of cell sheet engineering [24, 40]. It is also important to note that several factors can play a role in affecting the mechanical properties of VSMC sheets, such as culture period, ascorbic acid treatment as we have found in this study.

3.3. Stacking nonpatterned or patterned VSMC sheet into bilayer VSMC patches.

To generate bilayer VSMC patches, each VSMC sheets were prepared on CMCty and Alty hydrogel substrates. Once VSMC sheets were prepared on two different types of hydrogel substrates, they were stacked to generate bilayer VSMC patches in a similar strategy to that of transferring monolayer VSMC sheets (Figure 1). To validate the stacking strategy, we performed a lap shear test to confirm if our stacking strategy generates enough bonding between two layers of the bilayer VSMC patches to prevent layer delamination (Figure 6 and S4a). The bilayer VSMC patches incubated overnight after stacking showed strong bonding between two layers to exhibit cohesive failure from the lap shear test: the left and right substrate had clear presence of both green and red labeled VSMC sheets, indicating failure was cohesive rather than by layer delamination (adhesive) (Figure 6a). There were other cases showing complete detachment of bilayer VSMC patches from the hydrogel substrate without delamination supports strong interaction between layers even though force was not measured (Figure S4b). The control group showed no bonding between the two layers: the left substrate showed a non-damaged green-labeled VSMC sheet, and the right substrate showed a non-damaged red-labeled VSMC sheet, indicating detachment between individual layers (delamination) (Figure 6b). The measured maximum force showed 8.14 ± 3.32 mN for bilayer VSMC patches while the control (no incubation) showed no force being measured, as expected. The lap shear strength was calculated as,

$$Lap\ \ shear\ \ strength\ \ (Pa)\ \ = \frac{Maximum\ \ load\ \ force\ \ (N)}{Overlapping\ \ area\ \ (m^2)} \quad (6)$$

For bilayer patches, the overlapping area, in which the cell sheets are stacked, was determined to be 46.68 ± 12.00 mm^2, resulting in a lap shear strength (cohesive strength) of 169.79 ± 33.14 N/m^2 (Pa). Note that the actual bonding area (cell-cell contact area) could be much smaller. Further investigations are needed to elucidate the nature of the bonding.

Before proceeding with the mechanical property characterization of bilayer VSMC patches, the structure and collagen content were characterized. To mimic the distinct helical configurations of collagen fiber families seen in native tissue, two layers of patterned VSMC sheets were stacked at alternating angles to generate BTP, *i.e.* the pattern of top layer was in direction of −15°, and the pattern of bottom layers was in direction of +15° relative to x axis indicating 0°. As shown in Figure 7, the structure of each VSMC sheets was well-maintained after stacking. BNP showed randomly orientated morphology of cells, whereas BPP showed aligned structural orientation for green and red VSMC sheets in the same direction. BTP showed aligned structural orientation for both green (+15°) and red VSMC (−15°) sheets in different directions. Collagen staining also showed differences in structural organization of collagen fibers in the bilayer VSMC patches depending on the stacking direction (Figure 7b). While BPP showed the alignment of collagen fibers in one direction, BTP showed the alignment of collagen fibers in two directions (+15° and −15°), and BNP showed randomly dispersed collagen organization. As collagen is an abundant ECM in the blood vessel, collagen content was compared. The total amount of collagen (per sample) of the nonpatterned VSMC sheets was 18.95 ± 5.83 μg, which doubled when stacked to generate BNP to give 38.43 ± 2.24 μg. The patterned VSMC sheets was 11.23 ± 4.31 μg, which doubled to 23.87 ± 3.65μg when stacked to generate bilayer patterned VSMC patches. These results showed that ECM was neither damaged, nor lost during the stacking procedure. As shown in Figure 7c, the collagen normalized by a wet mass showed similar values of 7.07 ± 2.75 μg/mg ~ 7.78 ± 0.72 μg/mg (Figure 7c). In addition, collagen content of trypsin-treated VSMCs (1×10^6 cells) gave only 2.85 μg /mg. These results support our claim that harvesting cell sheets with our approach retains collagen while trypsin treatment does not, as trypsin is known to degrade cell-cell junctions and ECM by hydrolyzing proteins [64]. Interestingly, the staining results showed that the substrate patterns influenced cellular morphology and their organization; however, they did not affect collagen synthesis as shown by the consistent collagen content results. These results is consistent with previous reports from our lab of single non-patterned and patterned VSMC sheets grown on APTES-pNIPAAm [40] or polyethyleneimine (PEI) [24] coated substrates showing no difference in collagen or elastin production. Thus, our findings collectively indicate that the different mechanical behavior of VSMC sheets or VSMC patches is due to their structure, not their composition.

3.4. Prediction and characterization of bilayer VSMC patches mechanics.

To characterize the mechanical properties of bilayer vascular patches, various stacking and stretching directions of bilayer patterned VSMC patches (BP) were studied using a custom-built uniaxial tensile tester and finite element modeling (Figure 8). As shown in Figure 8, θ indicates the angle between the patterning direction of VSMC patches and the stretching direction. For example, θ = 0° means the patterning direction of VSMC patches is aligned to the stretching direction, and θ = 90° means the patterning direction is perpendicular to the stretching direction. Cauchy stress-stretch curves were obtained and compared against the model with goodness-of-fit/predict RMS assessment calculation in Figure 8. Engineering stress-strain curve for bilayer patterned VSMC patches were shown in Figure S5 as a comparison. Bilayer nonpatterned VSMC patches are shown in FigureS6. The results showed good agreement between simulation and experiment. For both BPP and BTP, lower θ tends to show steeper slope indicating a stiffer stress-stretch response when patterning was more aligned to the loading direction. Similar results were reported with collagen microfiber reinforced elastin-like protein sheet [65]. The designs in which two family of collagen fibers were more closely aligned to the loading direction (lower θ) tended to display a higher stiffness than the design where fibers are less aligned (higher θ).

Interestingly, mechanical results of monolayer VSMC sheet in Figure 5 showed higher failure stretch for patterned VSMC sheet when it is stretched in the perpendicular direction compared to parallel direction stretching. Similar results were previously reported by us and others, such as patterned VSMC sheets prepared on PNIPAAm grafted PDMS substrate [40], collagen microfiber reinforced elastin-like protein sheet [65], and human artery native tissue [66]. These results showed when fibers or patterning were more aligned to the loading direction, the samples showed enhanced stiffness, but lower stretch. The higher failure stretch when the samples were stretched in the perpendicular direction is possibly associated with collagen reorientation. When fibers or patterning were less aligned to the loading direction, collagen fibers were allowed to reorient in the direction of mechanical loading [19, 67, 68]. Nesbitt *et al.* reported that the collagen fibrils randomly aligned at the beginning oriented, and then began to straighten and gradually aligned in the direction of applied stress [19].

Although monolayer patterned VSMC sheets and bilayer patterned VSMC patches showed structural and mechanical behavior that mimics vascular tissue, further work is needed in order to successfully build engineered vascular patches. We recognize that the mechanical properties are driven by both cell and cell-derived extracellular matrix (ECM), and that VSMC sheets grown under different conditions (e.g., substrate, substrate surface coating, cell type, medium, and culture period) are expected to secrete ECM with different compositional and structural organization characteristics. Here, direct comparison of mechanical properties between monolayer and bilayer VSMC patches was not performed as the culture period differed for monolayer VSMC sheets (14 days) compared to bilayer VSMC patches (10 days). For bottom-up tissue engineering approach, future studies that allow direct mechanical comparison between monolayer and multilayer cell sheets grown under the same conditions may provide better insight for mechanical property prediction using the coupled experimental-computational approach. Also, multiple layers of VSMC

patch can be generated by multiplexing our stacking procedure. Briefly, multiple bi-layers can be cultured in parallel and then stacked to form thicker constructs – it may also be necessary to incorporate layers with capillary networks in thicker constructs to provide nutrients and remove waste. Futhermore, a layer consisting of an endothelial cell sheet could be incorporated into VSMC patches to mimic the endothelium or tunica intima, helping to prevent thrombosis. Ideally, an engineered vascular graft would need the support of an adventitial layer for additional mechanical support as well as providing nutriens via a capillary network. Direct omparison with native tissue, either with native aorta mechanics and ultimately an *in vivo* implantation and studies will further clarify the value of enzymatic substrate-based cell sheet engineering approach on vascular patch application. Such a tissue engineered vascular graft could be validated using our coupled experimental-computational approach.

4. Conclusion

In this study, we used enzymatically degradable hydrogel substrate to create patterned vascular smooth muscle cell sheets and evaluated their morphology, structure, and function. We observed good viability with the structural maintenance of the harvested cell sheet for an elongated culture period confirming the nondestructive detachment strategy. In addition, structural and mechanical properties of patterned VSMC sheets showed mechanical nonlinearity and anisotropy. Collagen characterization showed that patterning and stacking did not affect the collagen content, which revealed that the difference in mechanical properties between patterned and nonpatterned VSMC sheets is attributed to differences in structure but not composition. Moreover, as a biomimetic approach, patterned VSMC sheets can be stacked in different alternating angles to mimic the blood vessel structure and mechanical characterization. A finite-element computation model considering collagen fiber orientation was developed and showed good fitting and predicting capabilities. Results from our study suggest that an integrated approach of design, fabrication, testing, and computational modeling can be carried out iteratively to achieve a three-dimensional engineered vascular patch with desired mechanical function. These results demonstrate the feasibility of using enzymatically degradable hydrogel substrate for fabricating multiple layers of VSMC sheets and its potential as a building block for vascular patch development. Moreover, within the context of biomimetic approach, the results represent promising steps towards designing functional tissue engineered biomaterials through understanding the close correlation between structure and mechanics.

Supplementary Material

Refer to Web version on PubMed Central for supplementary material.

Acknowledgements

Nae Gyune Rim is an HHMI (Howard Hughes Medical Institute) international student research fellow. This work was supported by Boston Universtiy Undergraduate Research Opportunities Program (UROP) fellowship (to A.Y) and Supplemental Undergraduate Research Funds (SURF) (to A.Y), the Hartwell Foundation (to J.Y.W) and National Heart, Lung, and Blood Institute (NIH) research project grant No. R01 HL-098028 (to Y.Z),

References

[1]. Shin H, Jo S, Mikos AG. Biomimetic materials for tissue engineering. Biomaterials 2003;24:4353–64. [PubMed: 12922148]

[2]. Ma PX. Biomimetic materials for tissue engineering. Adv Drug Deliv Rev 2008;60:184–98. [PubMed: 18045729]

[3]. Langer R, Vacanti JP. Tissue engineering. Science 1993;260:920–6. [PubMed: 8493529]

[4]. Mann BK, West JL. Tissue engineering in the cardiovascular system: progress toward a tissue engineered heart. Anat Rec 2001;263:367–71. [PubMed: 11500813]

[5]. Salacinski HJ, Goldner S, Giudiceandrea A, Hamilton G, Seifalian AM, Edwards A, et al. The mechanical behavior of vascular grafts: a review. J Biomater Appl 2001;15:241–78. [PubMed: 11261602]

[6]. Kamenskiy AV, Pipinos II, MacTaggart JN, Kazmi SA, Dzenis YA. Comparative analysis of the biaxial mechanical behavior of carotid wall tissue and biological and synthetic materials used for carotid patch angioplasty. J Biomech Eng 2011;133:111008.

[7]. Schmedlen RH, Elbjeirami WM, Gobin AS, West JL. Tissue engineered small-diameter vascular grafts. Clin Plast Surg 2003;30:507–17. [PubMed: 14621299]

[8]. Kumar VA, Brewster LP, Caves JM, Chaikof EL. Tissue Engineering of Blood Vessels: Functional Requirements, Progress, and Future Challenges. Cardiovasc Eng Technol 2011;2:137–48. [PubMed: 23181145]

[9]. Rzucidlo EM, Martin KA, Powell RJ. Regulation of vascular smooth muscle cell differentiation. J Vasc Surg 2007;45 Suppl A:A25–32. [PubMed: 17544021]

[10]. Hahn C, Schwartz MA. Mechanotransduction in vascular physiology and atherogenesis. Nat Rev Mol Cell Biol 2009;10:53–62. [PubMed: 19197332]

[11]. Holzapfel GA, Gasser TC, Ogden RW. A New Constitutive Framework for Arterial Wall Mechanics and a Comparative Study of Material Models. Journal of elasticity and the physical science of solids 2000;61:1–48.

[12]. Brown BA, Williams H, George SJ. Evidence for the Involvement of Matrix-Degrading Metalloproteinases (MMPs) in Atherosclerosis. Prog Mol Biol Transl Sci 2017;147:197–237. [PubMed: 28413029]

[13]. Ponticos M, Partridge T, Black CM, Abraham DJ, Bou-Gharios G. Regulation of collagen type I in vascular smooth muscle cells by competition between Nkx2.5 and deltaEF1/ZEB1. Mol Cell Biol 2004;24:6151–61. [PubMed: 15226419]

[14]. Avolio A, Jones D, Tafazzoli-Shadpour M. Quantification of alterations in structure and function of elastin in the arterial media. Hypertension 1998;32:170–5. [PubMed: 9674656]

[15]. O'Connell MK, Murthy S, Phan S, Xu C, Buchanan J, Spilker R, et al. The three-dimensional micro- and nanostructure of the aortic medial lamellar unit measured using 3D confocal and electron microscopy imaging. Matrix Biol 2008;27:171–81. [PubMed: 18248974]

[16]. Solan A, Prabhakar V, Niklason L. Engineered vessels: importance of the extracellular matrix. Transplant Proc 2001;33:66–8. [PubMed: 11266708]

[17]. Miyazaki H, Hasegawa Y, Hayashi K. Tensile properties of contractile and synthetic vascular smooth muscle cells. Jsme Int J C-Mech Sy 2002;45:870–9.

[18]. Wagenseil JE, Mecham RP. Vascular extracellular matrix and arterial mechanics. Physiol Rev 2009;89:957–89. [PubMed: 19584318]

[19]. Nesbitt S, Scott W, Macione J, Kotha S. Collagen Fibrils in Skin Orient in the Direction of Applied Uniaxial Load in Proportion to Stress while Exhibiting Differential Strains around Hair Follicles. Materials 2015;8:1841–57. [PubMed: 28788035]

[20]. Chow MJ, Turcotte R, Lin CP, Zhang Y. Arterial extracellular matrix: a mechanobiological study of the contributions and interactions of elastin and collagen. Biophys J 2014;106:2684–92. [PubMed: 24940786]

[21]. Holzapfel GA, Sommer G, Gasser CT, Regitnig P. Determination of layer-specific mechanical properties of human coronary arteries with nonatherosclerotic intimal thickening and related

constitutive modeling. Am J Physiol Heart Circ Physiol 2005;289:H2048–58. [PubMed: 16006541]

[22]. Sarkar S, Dadhania M, Rourke P, Desai TA, Wong JY. Vascular tissue engineering: microtextured scaffold templates to control organization of vascular smooth muscle cells and extracellular matrix. Acta Biomater 2005;1:93–100. [PubMed: 16701783]

[23]. Brooke BS, Bayes-Genis A, Li DY. New Insights into Elastin and Vascular Disease. Trends in Cardiovascular Medicine 2003;13:176–81. [PubMed: 12837579]

[24]. Isenberg BC, Backman DE, Kinahan ME, Jesudason R, Suki B, Stone PJ, et al. Micropatterned cell sheets with defined cell and extracellular matrix orientation exhibit anisotropic mechanical properties. J Biomech 2012;45:756–61. [PubMed: 22177672]

[25]. Roberts EG, Lee EL, Backman D, Buczek-Thomas JA, Emani S, Wong JY. Engineering myocardial tissue patches with hierarchical structure-function. Ann Biomed Eng 2015;43:762–73. [PubMed: 25515314]

[26]. Nichol JW, Khademhosseini A. Modular Tissue Engineering: Engineering Biological Tissues from the Bottom Up. Soft Matter 2009;5:1312–9. [PubMed: 20179781]

[27]. Elbert DL. Bottom-up tissue engineering. Curr Opin Biotechnol 2011;22:674–80. [PubMed: 21524904]

[28]. Yamato M, Okano T. Cell sheet engineering. Materials Today 2004;7:42–7.

[29]. Kelm JM, Lorber V, Snedeker JG, Schmidt D, Broggini-Tenzer A, Weisstanner M, et al. A novel concept for scaffold-free vessel tissue engineering: self-assembly of microtissue building blocks. J Biotechnol 2010;148:46–55. [PubMed: 20223267]

[30]. Patel NG, Zhang G. Responsive systems for cell sheet detachment. Organogenesis 2013;9:93–100. [PubMed: 23820033]

[31]. Yang J, Yamato M, Shimizu T, Sekine H, Ohashi K, Kanzaki M, et al. Reconstruction of functional tissues with cell sheet engineering. Biomaterials 2007;28:5033–43. [PubMed: 17761277]

[32]. Yang J, Yamato M, Kohno C, Nishimoto A, Sekine H, Fukai F, et al. Cell sheet engineering: Recreating tissues without biodegradable scaffolds. Biomaterials 2005;26:6415–22. [PubMed: 16011847]

[33]. Williams C, Xie AW, Yamato M, Okano T, Wong JY. Stacking of aligned cell sheets for layer-by-layer control of complex tissue structure. Biomaterials 2011;32:5625–32. [PubMed: 21601276]

[34]. Isenberg BC, Tsuda Y, Williams C, Shimizu T, Yamato M, Okano T, et al. A thermoresponsive, microtextured substrate for cell sheet engineering with defined structural organization. Biomaterials 2008;29:2565–72. [PubMed: 18377979]

[35]. Jun I, Kim SJ, Lee J-H, Lee YJ, Shin YM, Choi E, et al. Transfer Printing of Cell Layers with an Anisotropic Extracellular Matrix Assembly using Cell-Interactive and Thermosensitive Hydrogels. Adv Funct Mater 2012;22:4060–9.

[36]. Tekin H, Ozaydin-Ince G, Tsinman T, Gleason KK, Langer R, Khademhosseini A, et al. Responsive Microgrooves for the Formation of Harvestable Tissue Constructs. Langmuir 2011;27:5671–9. [PubMed: 21449596]

[37]. Williams C, Tsuda Y, Isenberg BC, Yamato M, Shimizu T, Okano T, et al. Aligned Cell Sheets Grown on Thermo-Responsive Substrates with Microcontact Printed Protein Patterns. Advanced Materials 2009;21:2161–4.

[38]. Lee EL, Bendre HH, Robinson MK, Wong JY. Modulating Alignment and Contractile Protein Expression in Vascular Smooth Muscle Cell Sheets Using Microcontact Printing and Mechanical Conditioning. Northeast Bioengin C 2014.

[39]. Chang S, Song S, Lee J, Yoon J, Park J, Choi S, et al. Phenotypic modulation of primary vascular smooth muscle cells by short-term culture on micropatterned substrate. PLoS One 2014;9:e88089. [PubMed: 24505388]

[40]. Backman DE, LeSavage BL, Shah SB, Wong JY. A Robust Method to Generate Mechanically Anisotropic Vascular Smooth Muscle Cell Sheets for Vascular Tissue Engineering. Macromol Biosci 2017;17.

[41]. Akintewe OO, Roberts EG, Rim NG, Ferguson MAH, Wong JY. Design Approaches to Myocardial and Vascular Tissue Engineering. Annu Rev Biomed Eng 2017;19:389–414. [PubMed: 28471698]

[42]. Chen G, Qi Y, Niu L, Di T, Zhong J, Fang T, et al. Application of the cell sheet technique in tissue engineering. Biomed Rep 2015;3:749–57. [PubMed: 26623011]

[43]. Jin R, Hiemstra C, Zhong Z, Feijen J. Enzyme-mediated fast in situ formation of hydrogels from dextran-tyramine conjugates. Biomaterials 2007;28:2791–800. [PubMed: 17379300]

[44]. Kurisawa M, Chung JE, Yang YY, Gao SJ, Uyama H. Injectable biodegradable hydrogels composed of hyaluronic acid-tyramine conjugates for drug delivery and tissue engineering. Chem Commun (Camb) 2005:4312–4. [PubMed: 16113732]

[45]. Ogushi Y, Sakai S, Kawakami K. Synthesis of enzymatically-gellable carboxymethylcellulose for biomedical applications. J Biosci Bioeng 2007;104:30–3. [PubMed: 17697980]

[46]. Sakai S, Kawakami K. Synthesis and characterization of both ionically and enzymatically cross-linkable alginate. Acta Biomaterialia 2007;3:495–501. [PubMed: 17275429]

[47]. Ogushi Y, Sakai S, Kawakami K. Phenolic hydroxy groups incorporated for the peroxidase-catalyzed gelation of a carboxymethylcellulose support: cellular adhesion and proliferation. Macromol Biosci 2009;9:262–7. [PubMed: 19089866]

[48]. Sakai S, Hirose K, Moriyama K, Kawakami K. Control of cellular adhesiveness in an alginate-based hydrogel by varying peroxidase and H(2)O(2) concentrations during gelation. Acta Biomater 2010;6:1446–52. [PubMed: 19818883]

[49]. Sakai S, Ogushi Y, Kawakami K. Enzymatically crosslinked carboxymethylcellulose-tyramine conjugate hydrogel: cellular adhesiveness and feasibility for cell sheet technology. Acta Biomater 2009;5:554–9. [PubMed: 19010747]

[50]. Kim JJ. Enzymatically degradable hydrogel platform for cell sheet engineering [unpublished doctoral thesis]: Boston University; 2015.

[51]. Rim N, Kim J, Wong J. Fabrication of Vascular Smooth Muscle Cell Sheets using an Enzymatic Sacrificial Hydrogel System. Tissue Eng Pt A 2015;21:S28–S.

[52]. Camelliti P, Gallagher JO, Kohl P, McCulloch AD. Micropatterned cell cultures on elastic membranes as an in vitro model of myocardium. Nat Protoc 2006;1:1379–91. [PubMed: 17406425]

[53]. Rensen SS, Doevendans PA, van Eys GJ. Regulation and characteristics of vascular smooth muscle cell phenotypic diversity. Neth Heart J 2007;15:100–8. [PubMed: 17612668]

[54]. Beamish JA, He P, Kottke-Marchant K, Marchant RE. Molecular regulation of contractile smooth muscle cell phenotype: implications for vascular tissue engineering. Tissue Eng Part B Rev 2010;16:467–91. [PubMed: 20334504]

[55]. Backman DE, LeSavage BL, Wong JY. Versatile and inexpensive Hall-Effect force sensor for mechanical characterization of soft biological materials. J Biomech 2017;51:118–22. [PubMed: 27923480]

[56]. O'Connell MK, Murthy S, Phan S, Xu C, Buchanan J, Spilker R, et al. The three-dimensional micro- and nanostructure of the aortic medial lamellar unit measured using 3D confocal and electron microscopy imaging. Matrix Biol 2008;27:171–81. [PubMed: 18248974]

[57]. Gasser TC, Ogden RW, Holzapfel GA. Hyperelastic modelling of arterial layers with distributed collagen fibre orientations. J R Soc Interface 2006;3:15–35. [PubMed: 16849214]

[58]. Wagner HP, Humphrey JD. Differential passive and active biaxial mechanical behaviors of muscular and elastic arteries: basilar versus common carotid. J Biomech Eng 2011;133:051009.

[59]. Zeinali-Davarani S, Wang Y, Chow MJ, Turcotte R, Zhang Y. Contribution of collagen fiber undulation to regional biomechanical properties along porcine thoracic aorta. J Biomech Eng 2015;137:051001.

[60]. Curtis A, Riehle M. Tissue engineering: the biophysical background. Phys Med Biol 2001;46:R47–65. [PubMed: 11324976]

[61]. Chamley JH, Campbell GR, McConnell JD, Groschel-Stewart U. Comparison of vascular smooth muscle cells from adult human, monkey and rabbit in primary culture and in subculture. Cell Tissue Res 1977;177:503–22. [PubMed: 402216]

[62]. Jones BA, Aly HM, Forsyth EA, Sidawy AN. Phenotypic characterization of human smooth muscle cells derived from atherosclerotic tibial and peroneal arteries. J Vasc Surg 1996;24:883–91. [PubMed: 8918338]

[63]. Agrawal A, Lee BH, Irvine SA, An J, Bhuthalingam R, Singh V, et al. Smooth Muscle Cell Alignment and Phenotype Control by Melt Spun Polycaprolactone Fibers for Seeding of Tissue Engineered Blood Vessels. Int J Biomater 2015;2015:434876.

[64]. Kushida A, Yamato M, Konno C, Kikuchi A, Sakurai Y, Okano T. Decrease in culture temperature releases monolayer endothelial cell sheets together with deposited fibronectin matrix from temperature-responsive culture surfaces. J Biomed Mater Res 1999;45:355–62. [PubMed: 10321708]

[65]. Caves JM, Cui W, Wen J, Kumar VA, Haller CA, Chaikof EL. Elastin-like protein matrix reinforced with collagen microfibers for soft tissue repair. Biomaterials 2011;32:5371–9. [PubMed: 21550111]

[66]. Holzapfel GA, Sommer G, Regitnig P. Anisotropic mechanical properties of tissue components in human atherosclerotic plaques. J Biomech Eng 2004;126:657–65. [PubMed: 15648819]

[67]. Sasazaki Y, Shore R, Seedhom BB. Deformation and failure of cartilage in the tensile mode. J Anat 2006;208:681–94. [PubMed: 16761971]

[68]. Purslow PP, Bigi A, Ripamonti A, Roveri N. Collagen Fiber Reorientation around a Crack in Biaxially Stretched Aortic Media. Int J Biol Macromol 1984;6:21–5.

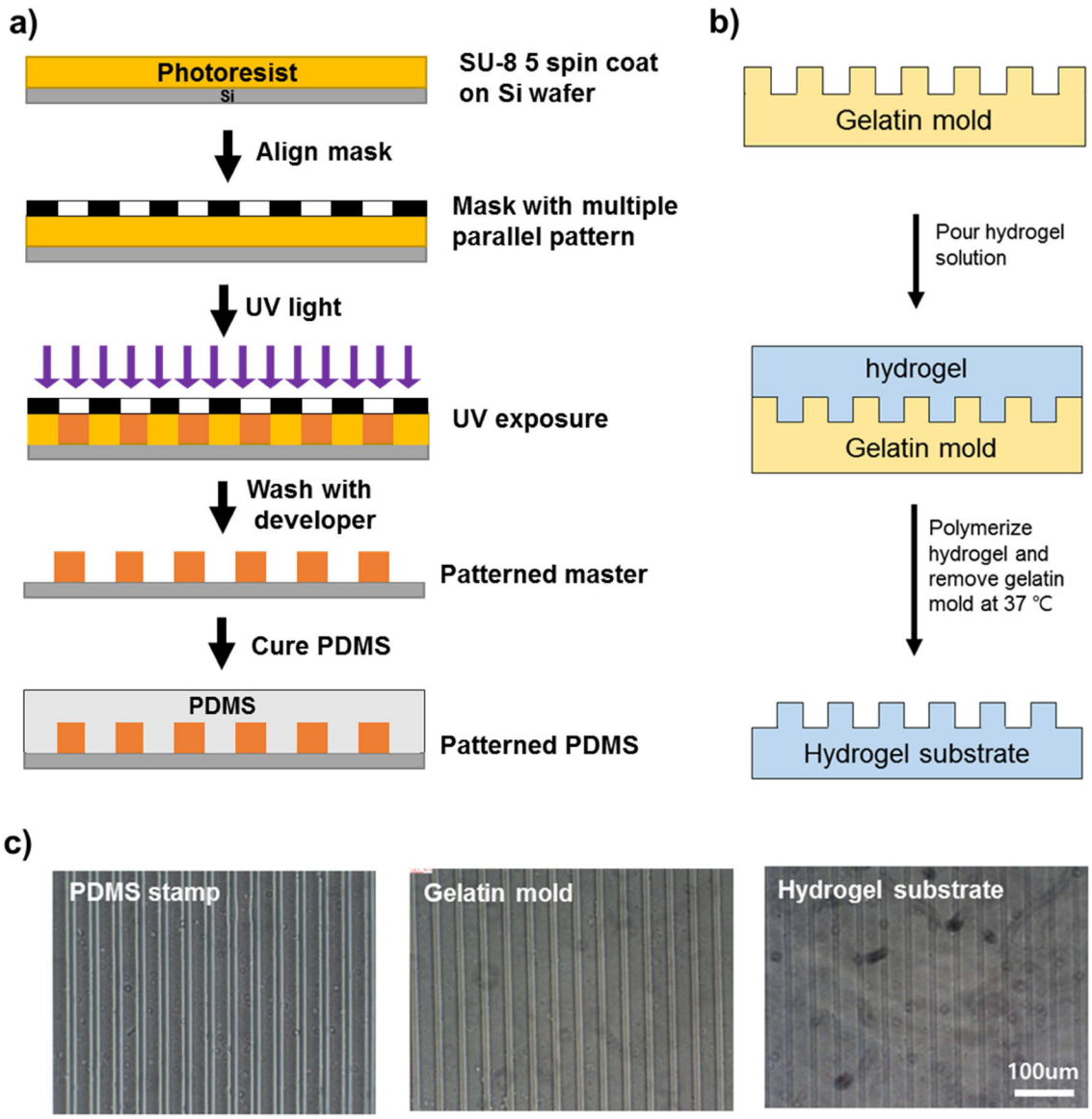

Scheme 1.

Fabrication of patterned hydrogel substrate using photolithography. a) Micro-patterning on silicon wafer via photolithography and PDMS preparation; b) Hydrogel substrate fabrication using gelatin mold stamped against PDMS; and c) Microscopic images showing pattern maintenance through PDMS stamp - Gelatin mold - Hydrogel substrate.

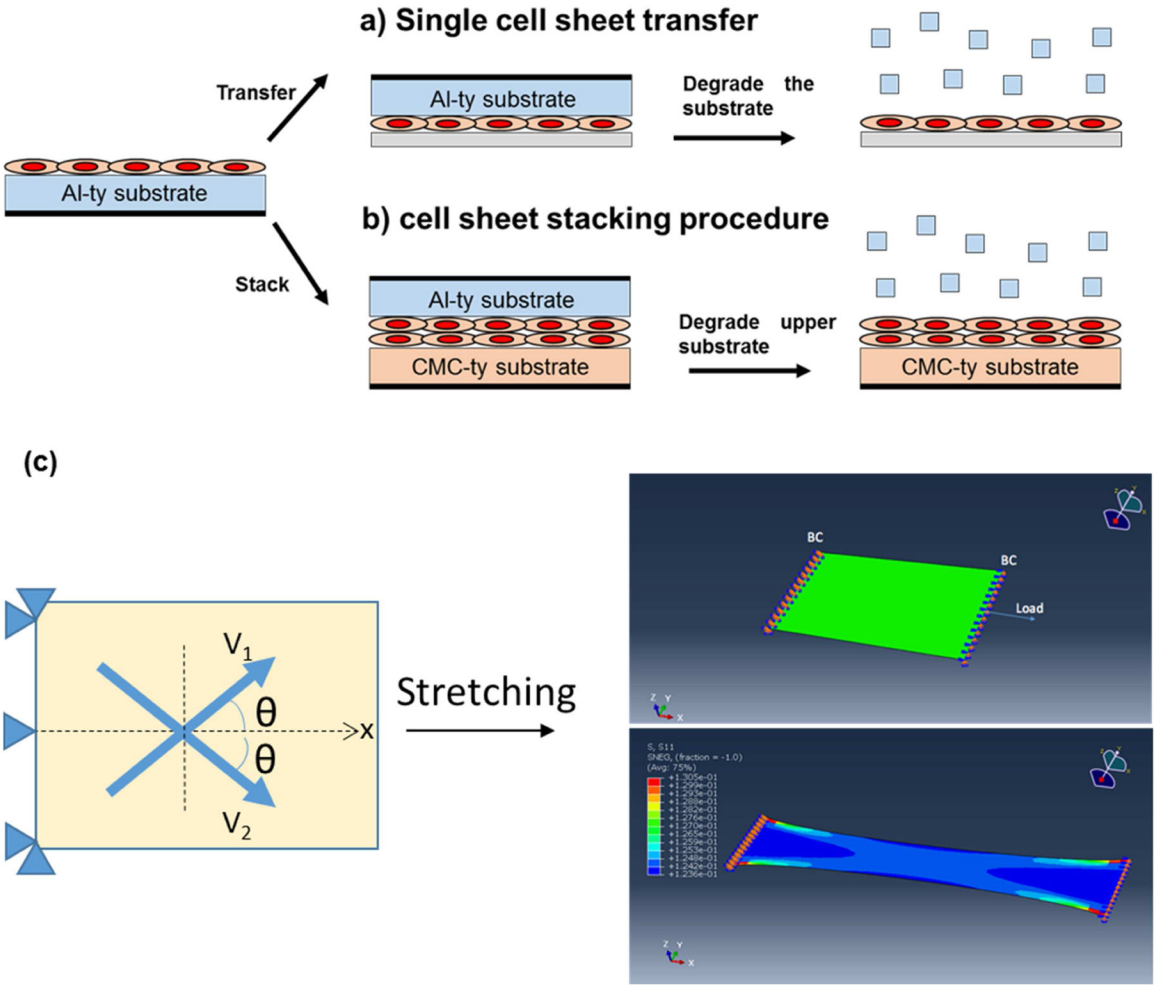

Figure 1.

Schematic of (a) VSMC sheet harvesting via enzymatic degradation of hydrogel substrate as monolayer and (b) VSMC sheet stacking strategy to fabricate bilayer. (c) Schematic showing bilayer VSMC patches mechanical stretching model. Reference vector (V_1, V_2) indicating two collagen fiber family orientation with respect to the stretching direction (x). A finite element model was developed to simulate uniaxial tensile testing of bilayer VSMC patches. Top panel: undeformed, bottom panel: deformed.

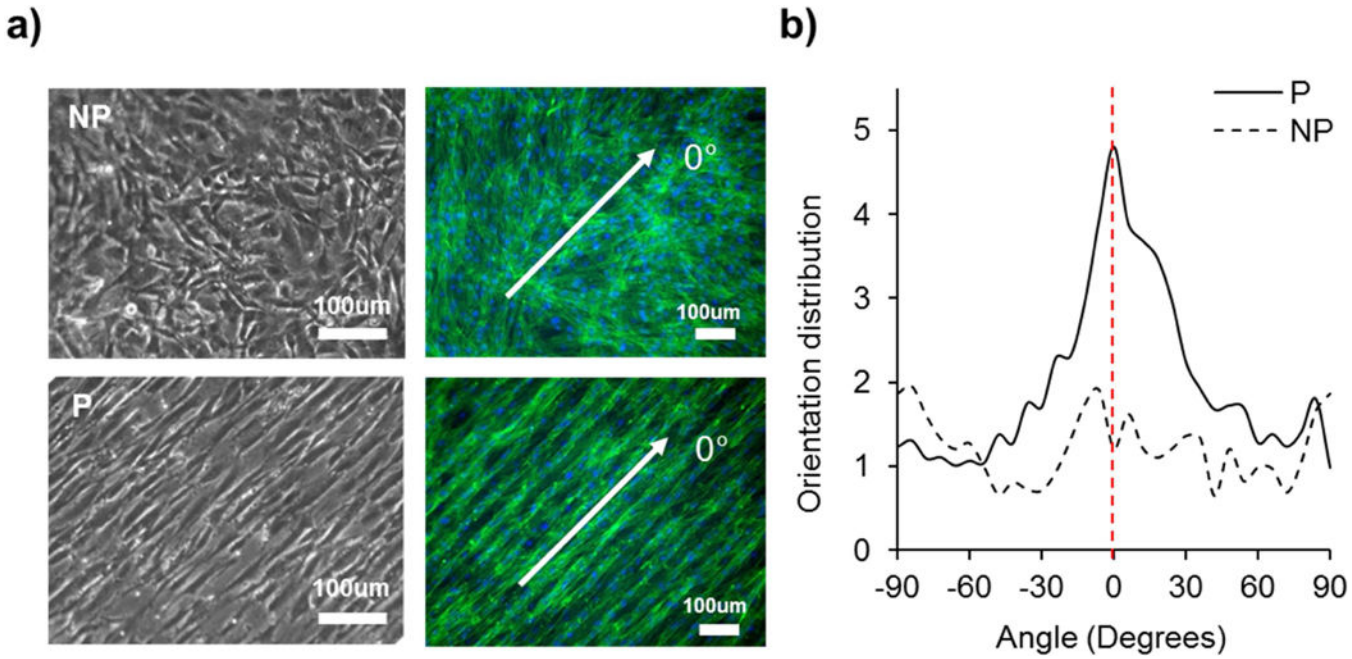

Figure 2.

Patterning of hydrogel substrate regulated cellular alignment. (a) Microscopic (left) and F-actin stained images (right) of cells grown on nonpatterned and patterned hydrogel. Green indicates actin filament and blue indicates nuclei. (b) F-actin stained images were further analyzed using 2D FFT alignment analysis. Cells grown on patterned hydrogel showed guided cellular alignment in the direction parallel to the pattern while cells grown on nonpatterned hydrogel showed random direction. White arrow in (a) indicates the direction of substrate patterning, where its angle is 0°, shown as the red dotted line in (b).

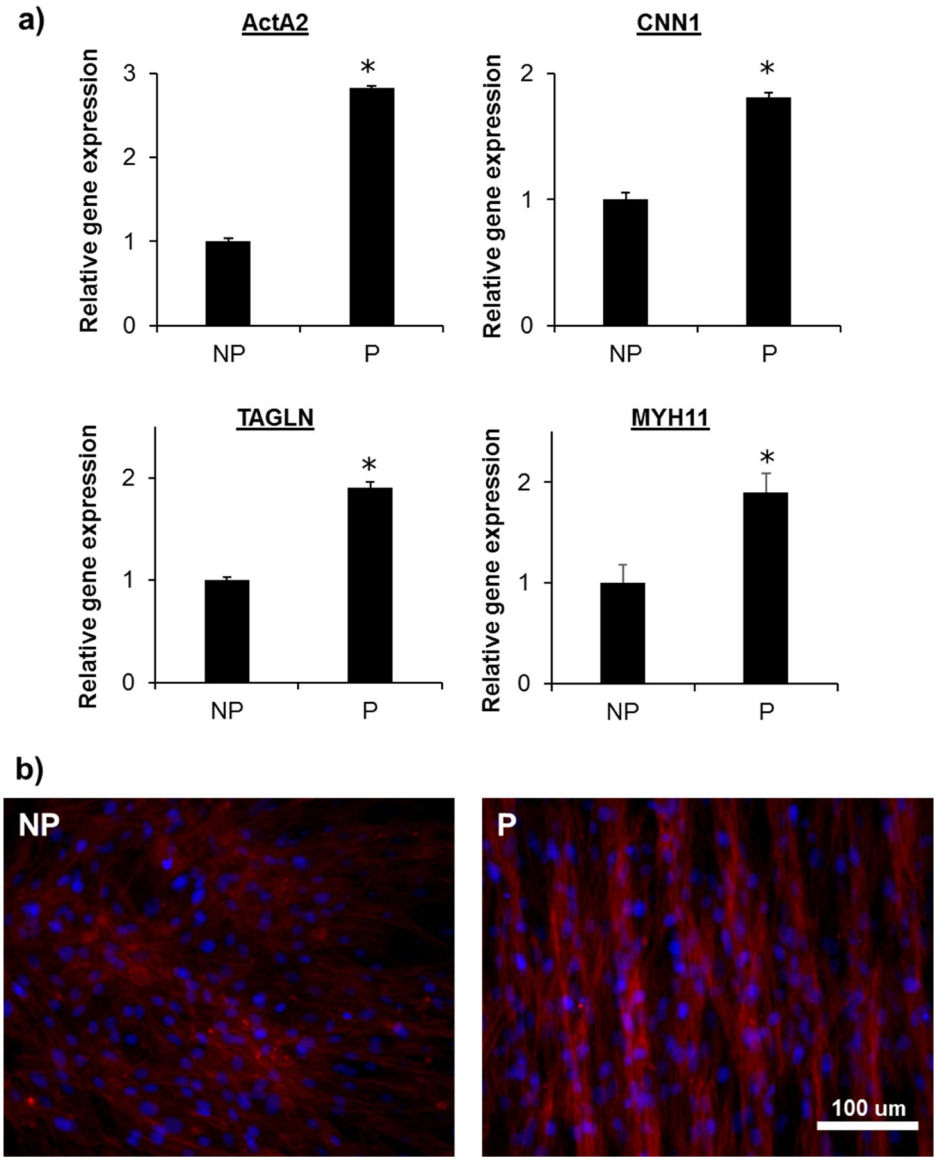

Figure 3.

Effect of cellular alignment on contractile marker expression. (a) Gene expression analysis using TaqMan assay. Relative gene expression level was normalized by GAPDH as housekeeping gene and NP as control. ($n=3$; *, $p<0.05$) (b) Smooth muscle myosin heavy chain (SM-MHC or MYH11) immunofluorescence stained VSMC sheet images. Red indicates SM-MHC and blue indicates nuclei. Scale bar 100 μm.

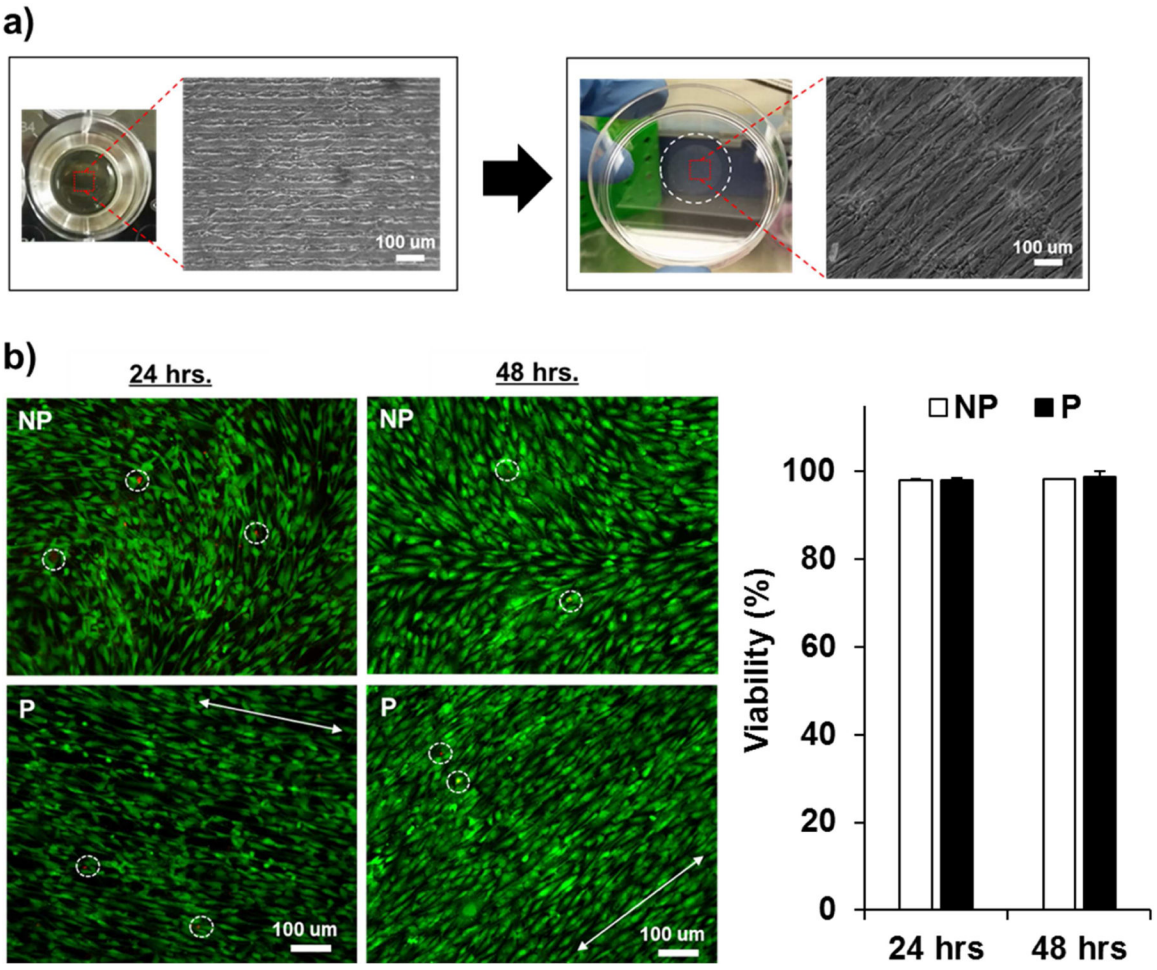

Figure 4.

Viability of harvested VSMC sheets. (a) Microscopic images of VSMC sheet before and after transfer showing maintenance of the circular shape of cell sheet and cellular alignment. (b) Live/Dead® cell viability assay of harvested VSMC sheet after 24 hrs and 48 hrs (*n=3*) shows that VSMC sheet is successfully harvested and transferred to the other substrate without cellular damage. Scale bar 100 μm.

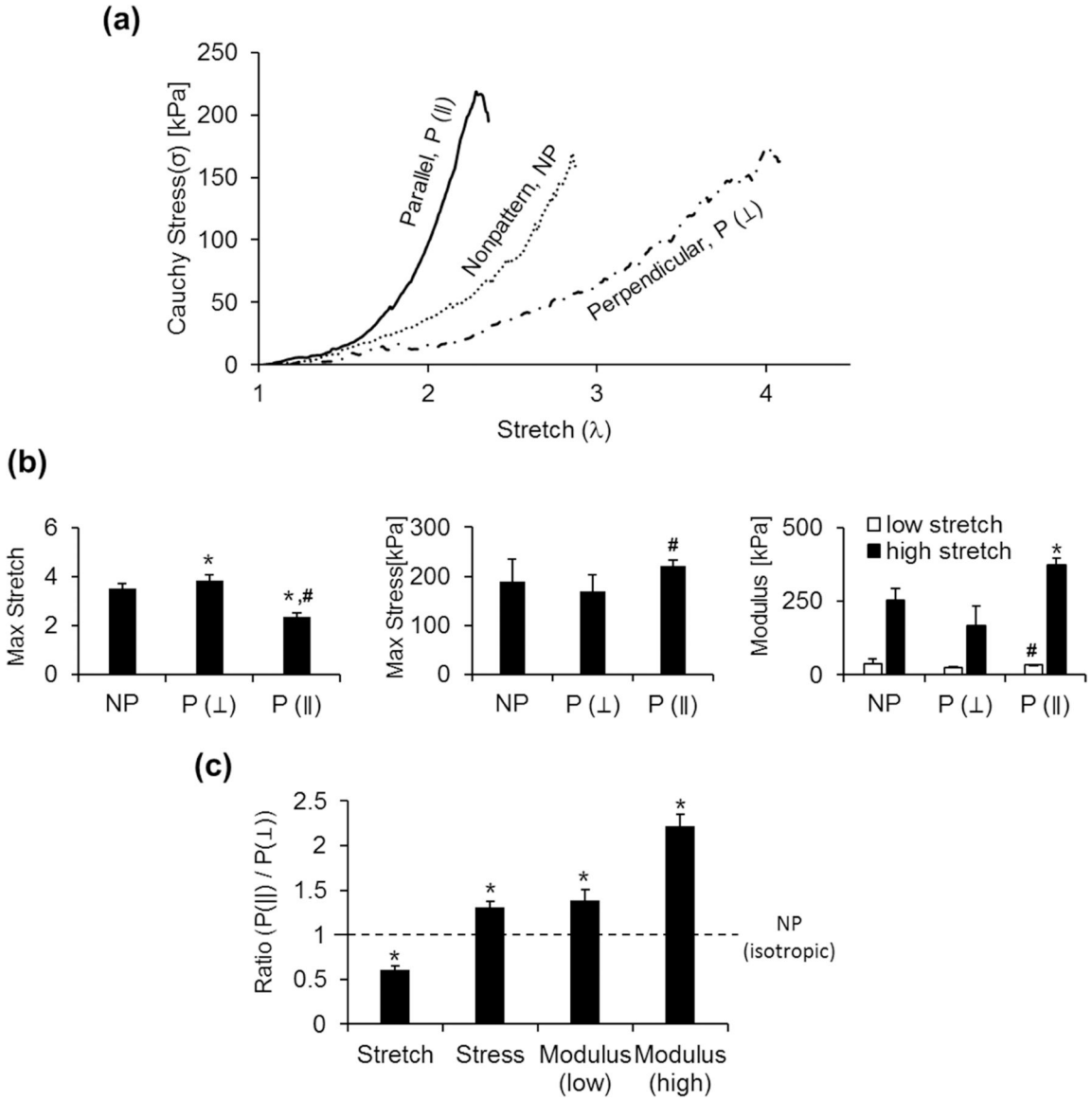

Figure 5.

Mechanical nonlinearity and anisotropy of patterned VSMC sheets. a) Representative Cauchy stress-stretch curve of a monolayer VSMC sheets. b) Max stretch, max stress, tensile modulus at low and high stretch was analyzed based on the stress-stretch results. c) Normalized ratio of the mechanical properties to better quantify anisotropic mechanical behavior. Ratio=1 indicates isotropic behavior. *n=3, *, relative to NP (P<0.05), # relative to P (⊥) (P<0.05)*

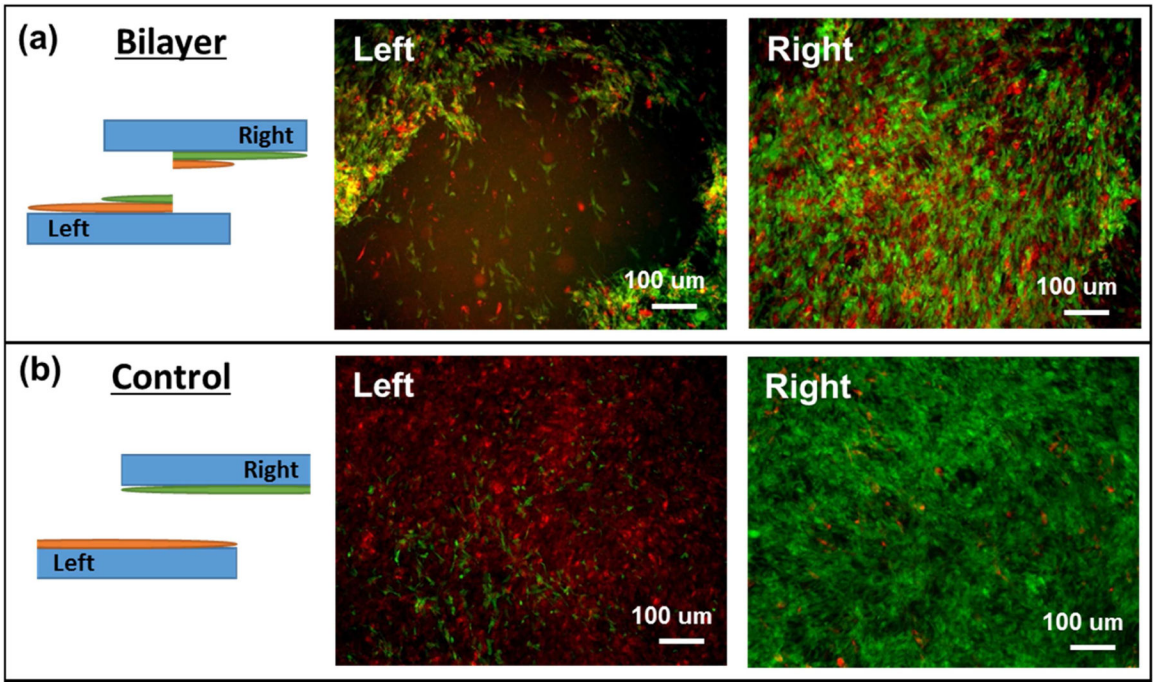

Figure 6.

VSMC sheet lap shear test between stacked layers. (a) Bilayer indicates overnight incubation after stacking and (b) control indicates no incubation after stacking. Prior to stacking, each VSMC sheet was pre-labeled with red (bottom layer) and green (top layer) cell tracker. Left and Right images were taken from the left (bottom) and right (top) cell sheet/substrate construct after the lap shear test. Scale bars represent 100 μm.

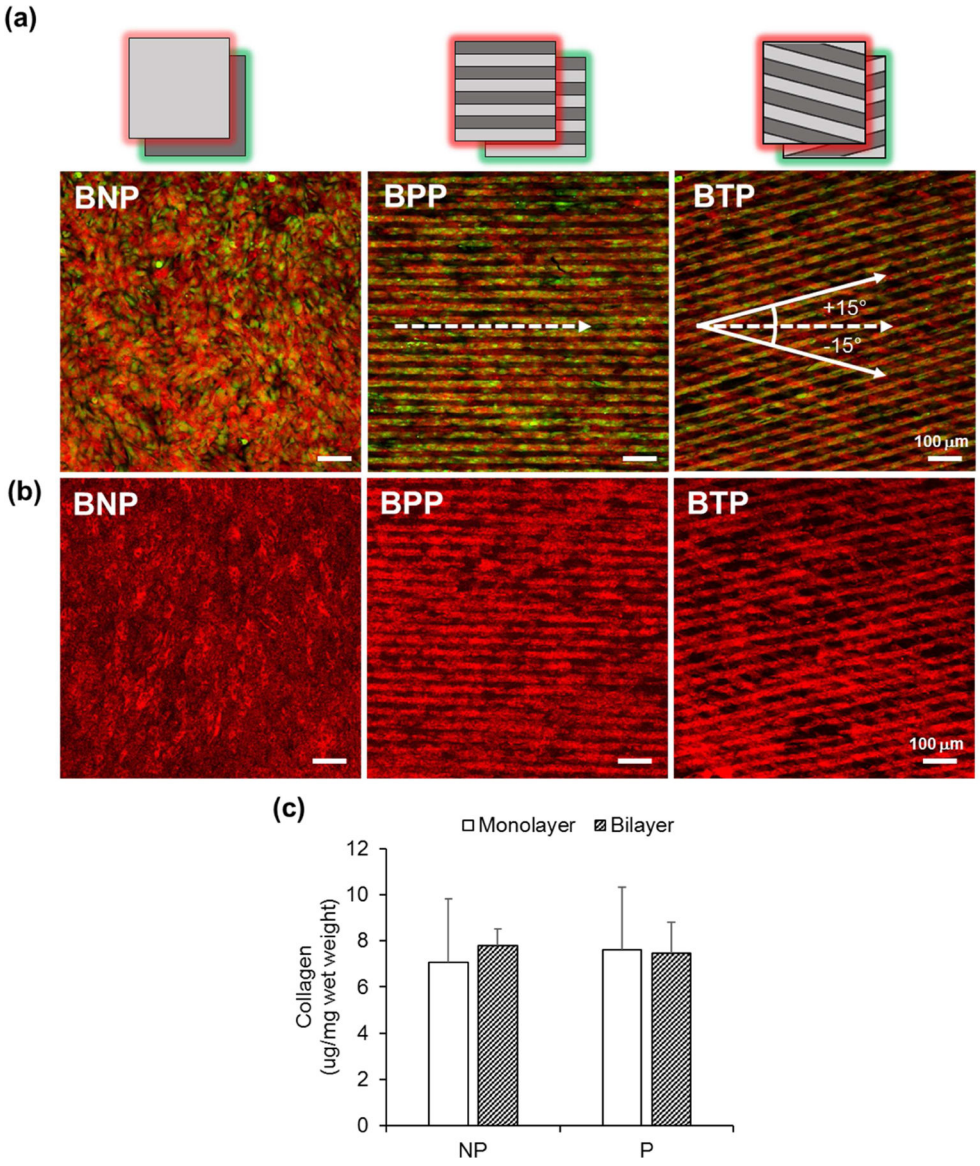

Figure 7.

Bilayer VSMC patches layered at alternating angles to mimic native tissue organization. BNP (Bilayer NonPatterned VSMC patches), BPP (Bilayer Parallel Patterned VSMC patches), BTP (Bilayer Tilted Patterned VSMC patches, bottom layer: +15°, top layer: −15°). (a) Cell tracker- labeled layers (Red for top layer, Green for bottom layer) prior to stacking for visualization. (b) Immunofluorescent collagen stained bilayer VSMC patches shown in red. (c) Normalized collagen content of monolayer and bilayer VSMC patches. n=3, *, P<0.05. Scale bars represent 100 μm.

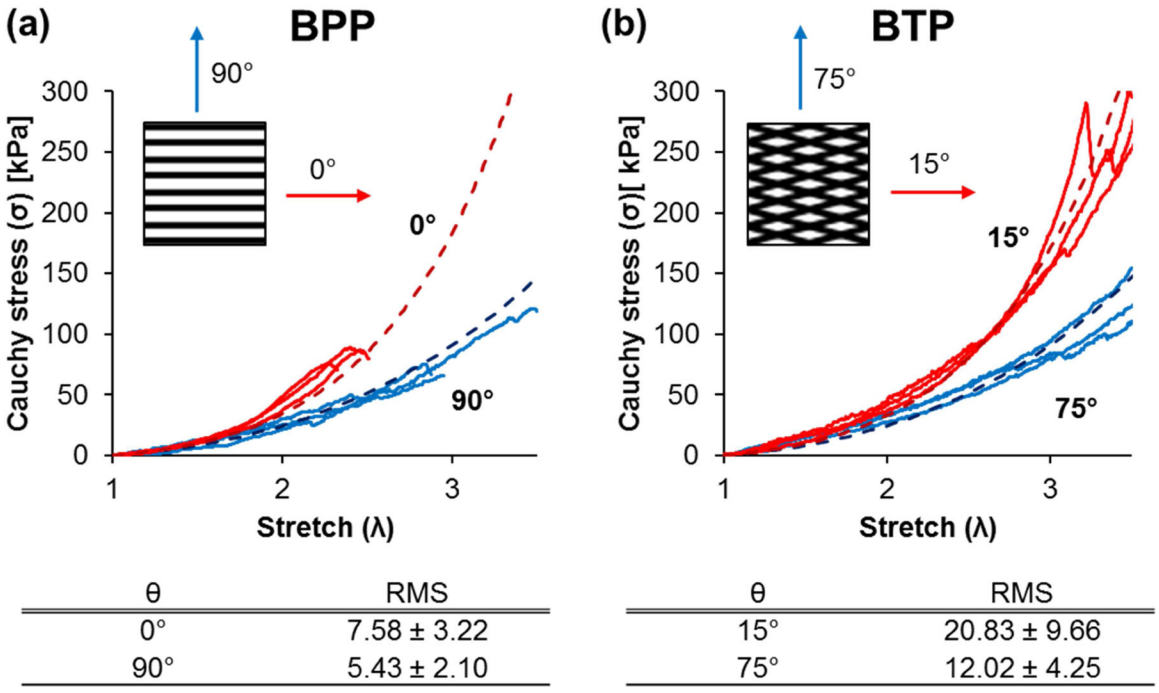

θ	RMS
0°	7.58 ± 3.22
90°	5.43 ± 2.10

θ	RMS
15°	20.83 ± 9.66
75°	12.02 ± 4.25

Figure 8.

Cauchy stress vs. stretch of (a) stacked bilayer patterned VSMC patches stretched in the direction where θ is 0° or 90°, and (b) stacked bilayer tilted patterned VSMC patches stretched in the direction where θ is 15° or 75°. Experimental data (solid lines) was compared to computational modeling (dotted lines) with goodness-of-fit/predict RMS shown on the bottom.

Table 1.

Components used to synthesize tyramine conjugated carboxymethyl cellulose (CMCty) and alginate (Alty).

	CMCty	Alty
MES (pH 6.0)	120 ml (0.05 M)	120 ml (0.1 M)
Sodium carboxymethyl cellulose	1.2 g	-
Alginate sodium salt	-	0.6 g
Tyramine hydrochloride	0.858 g	5.4 g
NHS	0.057 g	0.870 g
HOBt	0.134 g	-
EDC	0.473 g	2.899 g